Measurement of the rate of formation of pi-mu atoms in K_L^0 decay

S. H. Aronson,[a] R. H. Bernstein,[b,*] G. J. Bock,[c,†] R. D. Cousins, Jr.,[c,‡] J. F. Greenhalgh,[c,§] D. Hedin,[d,**] M. Schwartz,[c,††] T. K. Shea,[b,‡‡] G. B. Thomson,[d,§§] and B. Winstein[b]

[a]*Brookhaven National Laboratory, Upton, New York 11973*

[b]*University of Chicago, Chicago, Illinois 60637*

[c]*Stanford University, Stanford, California 94305*

[d]*University of Wisconsin, Madison, Wisconsin 53706*

(Received 13 January 1986)

Hydrogenlike atoms consisting of a pion and a muon can be formed in $K_L^0 \to \pi\mu\nu$ decays. In an experiment at Fermilab, 320 pi-mu atoms were detected and simultaneously the K_L^0 flux was monitored by recording ordinary $K_L^0 \to \pi\mu\nu$ decays. The first measurement of the branching ratio $R = \Gamma(K_L^0 \to \text{pi-mu atom} + \nu)/\Gamma(K_L^0 \to \pi\mu\nu) = (3.90 \pm 0.39) \times 10^{-7}$ is reported, based on a subset of 155 atoms. This ratio may be sensitive to anomalous interactions between the pion and the muon. In the absence of such interactions, theory predicts $R = (4.31 \pm 0.08) \times 10^{-7}$.

I. INTRODUCTION

In 1971, Nemenov[1] first considered the decay of the K_L^0 to a neutrino and a Coulomb-bound state consisting of a pion and a muon, the pi-mu atom. Several years later, in an experiment performed at Brookhaven National Laboratory, Coombes *et al.*[2,3] succeeded in detecting 18 examples of this rare decay. This sample of pi-mu atoms represented the first observation of an atom composed of two unstable particles and the first observation of an atomic decay of an elementary particle.

The properties of pi-mu atoms depend upon the nature of the π-μ interaction. Assuming that the interaction is purely electromagnetic, the pi-mu-atom's properties may be calculated by applying the same formalism used to describe the hydrogen atom. Since the pi-mu-atom's reduced mass is 60.13 MeV/c^2, about 120 times that of hydrogen, its Bohr radius is 120 times smaller and its binding energy 120 times greater. Whereas hydrogen is stable, the pi-mu atom should decay with a lifetime nearly equal to that of its shorter-lived constituent, the pion.

All hydrogenlike atoms, presumably including the pi-mu atom, may be described quite accurately using the nonrelativistic Schrödinger equation assuming a Coulomb potential. Relativistic corrections, however, contribute differently to the energy levels of pi-mu atoms than to those of hydrogen. These effects have been discussed at length in the literature.[4] For example, the $2P_{1/2}$-$2S_{1/2}$ splitting (the Lamb shift) is expected to be four orders of magnitude larger than in hydrogen and of opposite sign. This may be understood qualitatively as follows. Because of the smallness of the pi-mu-atom's Bohr radius, the pion and muon spend considerable time in the region in which the Coulomb potential is modified by the electron-positron vacuum polarization. This effect contributes 77.17×10^{-3} eV to a splitting of 79.45×10^{-3} eV in the pi-mu atom (neglecting pion size corrections), whereas in hydrogen it amounts to about 3% of 4.376×10^{-6} eV. Bar-Gadda and Cho[4] have calculated that an additional 0.5 to 1.0×10^{-3} eV is due to the finite size of the pion, which means that a measurement of the $2P_{1/2}$-$2S_{1/2}$ splitting accurate to a part in a thousand could provide an independent measurement of the pion charge radius.

The physics of the pi-mu atom is also reflected in the rate of formation of pi-mu atoms in K_L^0 decay, $\Gamma(K_L^0 \to (\pi\mu)_{\text{atom}}\nu)$. The calculation of this rate is outlined in Sec. II below. Because of the pointlike nature of the weak interaction, the rate depends directly upon the square of the pi-mu-atom wave function at zero separation, $|\psi(0)|^2$. A measurement of this formation rate can therefore be used as a probe of the short-range interactions between pions and muons. A deviation from the expected rate might signal the presence of an anomalous π-μ interaction. Staffin[5] examined various sources of such interactions and, using measurements of energy levels in muonic atoms and the measured muon $g-2$ value and capture rate, placed limits on any change to $|\psi(0)|^2$ from those sources.

In this paper we describe in detail an experiment performed at Fermilab in which we made the first measurement of the rate of formation of pi-mu atoms. Two-body $K_L^0 \to (\pi\mu)_{\text{atom}}\nu$ decays were detected while the K_L^0 flux was simultaneously measured by observing three-body $K_L^0 \to \pi\mu\nu$ ($K_{\mu 3}$) decays. The branching ratio

$$R \equiv \frac{\Gamma(K_L^0 \to (\pi\mu)_{\text{atom}}\nu)}{\Gamma(K_L^0 \to \pi\mu\nu)} \tag{1}$$

was then calculated, taking into account the relative detection efficiencies for the two decay modes. We compare our result to the current theoretical prediction for R. A brief account of this work has been published previously.[6] Further details may also be found in Ref. 7.

II. CALCULATION OF THE RATE OF FORMATION IN K_L^0 DECAY

The partial width for K_L^0 decay into the pi-mu-atom state of principal quantum number n, $(\pi\mu)_n$, is given by[8]

$$\Gamma(K_L^0\to(\pi\mu)_n\nu) = \frac{1}{2m_K}(2\pi)^4 |M|^2\delta^4(p_K-p_{\text{atom}}-p_\nu)d\omega_{\text{atom}}d\omega_\nu, \quad (2)$$

where $M=\langle(\pi\mu)_n\nu|H|K_L^0\rangle$ is the matrix element of the weak-interaction Hamiltonian H between initial and final states, and $p_i=(\mathbf{p}_i,p_i^0)$ is the four-momentum of particle i with $d\omega=d^3p_i/(2\pi)^3 2p_i^0$. This partial width has been calculated by several authors[1,5,9,10] and becomes, when summed over n,

$$\Gamma(K_L^0\to(\pi^+\mu^-)_{\text{atom}}\nu) = \frac{G_F^2\sin^2\theta_C(m_K^2-m_{\text{atom}}^2)^2}{16\pi m_K^3 m_\pi} \times[2m_\pi+m_\mu+\xi(q^2)m_\mu]^2|f_+(q^2)|^2 \times\sum_n|\psi_n(r=0)|^2. \quad (3)$$

G_F and θ_C are the Fermi coupling constant and the Cabibbo angle, while m denotes mass. The square of the Coulomb wave function evaluated at the origin is

$$|\psi_n(r=0)|^2=\left[\frac{\alpha m_\pi m_\mu}{n m_{\text{atom}}}\right]^3\frac{1}{\pi}, \quad (4)$$

where α is the fine-structure constant. Summing over final states of principal quantum number n increases the rate by about 20%:

$$\sum_{n=1}^{\infty}\frac{1}{n^3}\approx 1.2 .$$

The decay rate depends upon the hadronic part of the matrix element through the $K_{\mu3}$ form factors $f_+(q^2)$ and $f_-(q^2)$, which are found experimentally to depend linearly upon q^2 as follows:[11]

$$f_\pm(q^2)=f_\pm(0)(1+\lambda_\pm q^2/m_\pi^2), \qquad \xi(q^2)\equiv\frac{f_-(q^2)}{f_+(q^2)}, \quad (5)$$

where $q^2\equiv(p_K-p_\pi)^2=0.092$ (GeV/c^2)^2 for atom formation.

It is convenient to normalize the decay rate to pi-mu atoms by the $K_{\mu3}$ decay rate. The partial width for $K_L^0\to\pi\mu\nu$ decays may be written[12]

$$\Gamma(K_L^0\to\pi^+\mu^-\nu)=\frac{G_F^2\sin^2\theta_C m_K^5}{16\pi^3}|f_+(0)|^2\times10^{-2} \times\Big[0.9255+0.4221\lambda_+(m_K^2/m_\pi^2)-0.1900[1-\xi(0)] -0.0544[1-\xi(0)](m_K^2/m_\pi^2)\left[\lambda_+ +\frac{\lambda_+-\xi(0)\lambda_-}{1-\xi(0)}\right]+0.0219[1-\xi(0)]^2 +0.0141[1-\xi(0)](m_K^2/m_\pi^2)[\lambda_+-\xi(0)\lambda_-]\Big]. \quad (6)$$

The factor $G_F^2\sin^2\theta_C|f_+(0)|^2$ then cancels in forming the ratio R given by Eq. (1).

Four corrections to the value of R have been calculated. The effects of the finite size of the pion, vacuum polarization, and the first-order relativistic correction to the atomic wave function lower the decay rate to pi-mu atoms by 0.4%, 0.2%, and 3.8%, respectively,[10] while radiative corrections increase the $K_L^0\to\pi\mu\nu$ width by 2.1%.[13] The ratio R can then be expressed as a function of the $K_{\mu3}$ form factors and written to first order as

$$R=4.31[1.05+0.33\xi(0)](0.85+4.05\lambda_+)\times10^{-7}. \quad (7)$$

Using the world averages[11] of $\xi(0)=-0.11\pm0.09$ and $\lambda_+=0.034\pm0.005$ (λ_- is consistent with zero) with a correlation of $d\xi(0)/d\lambda_+=-14$, the predicted value of R is

$$R=(4.31\pm0.08)\times10^{-7}. \quad (8)$$

The quoted error is determined by propagating the correlated errors on the form factors.[14]

III. EXPERIMENTAL TECHNIQUE AND APPARATUS

A. Overview

Because the pi-mu-atom branching ratio was expected to be small, $\sim10^{-7}$, the experiment could not have been performed in a reasonable time without an intense source of decaying kaons. More important, the experiment could not have been performed at all without an efficient means of detecting pi-mu atoms and separating them unambiguously from $K_L^0\to\pi\mu\nu$ decays. Before describing the apparatus and our experimental technique in detail, we outline the way in which we addressed these two requirements.

The source of kaons was a large solid-angle neutral beam produced by high-energy protons incident upon a beryllium target. Our detector was sensitive to decays that occurred within a 250-m-long stretch of the neutral beam (the decay region). Pi-mu atoms produced in K_L^0 decays with sufficient momentum transverse to the K_L^0 direction emerged from the beam and were detected. The

beam traveled in an uninterrupted vacuum outside the detection apparatus in order to minimize the flux of secondary particles from interactions of beam particles with air.

Figure 1 shows the detection apparatus. The last ten meters of the decay region contained a system of magnets and a thin foil which allowed us to dissociate (ionize) pi-mu atoms and separate their constituents, the pion and muon. The neutral atoms traveled undeflected through magnet V, which bent charged tracks (e.g., unbound pions and muons) vertically. A thin aluminum foil, mounted vertically just above the neutral beam, ionized the atoms. Calculations have shown that approximately 0.01 in. of aluminum is sufficient to ionize a pi-mu atom.[9] We collected roughly half of our data with a 0.020-in. aluminum foil and the remainder with a 0.035-in. aluminum foil to allow verification that in each sample all the atoms were dissociated. After passage through the foil, the two charged particles traveled essentially collinearly and with the same velocity, since they originated in a bound state and the impulse required to separate them was negligible compared to the laboratory momentum of the atom. A horizontally deflecting magnet (magnet H) then separated the oppositely charged constituents in the plan view. The pion and muon emerged from the vacuum region through a thin window and traversed a magnetic spectrometer followed by particle identification elements.

Similarly, photons could convert in the foil and produce e^+e^- pairs. The e^+ and the e^- would also emerge from the foil nearly collinear (although typically not at the same velocity) and be separated by magnet H.

This arrangement of foil and magnets yielded two distinct classes of events, as illustrated in Fig. 2. States which were neutral when they passed through magnet V and then ionized (pi-mu atoms) or converted (photons) in the foil produced tracks in the spectrometer which, due to magnet H, lay in a plane. Such states yielded two track projections in the plan (top) view with an apparent vertex in magnet H but only one track projection in the elevation (side) view. Events with this topology were called "foil" events. States consisting of separate charged particles upstream of magnet V (such as ordinary K_L^0 decays) produced tracks in the apparatus which were separated in *both* projections by the combined effects of magnet V and magnet H. Such nonplanar topologies, with two or more track projections in each view, were called "nonfoil" events.

The data-acquisition trigger used two hodoscopes of horizontal scintillation counters (W and H) to distinguish the two classes of events: foil events were required to have exactly one struck counter in each hodoscope while nonfoil events were allowed one or more in each. To further simplify the identification of foil events, we operated the main spectrometer magnet, magnet A, with a field integral equal in magnitude to that of magnet H, but with opposite polarity. This arrangement restored the parallelism of the trajectories of the charged particles of foil

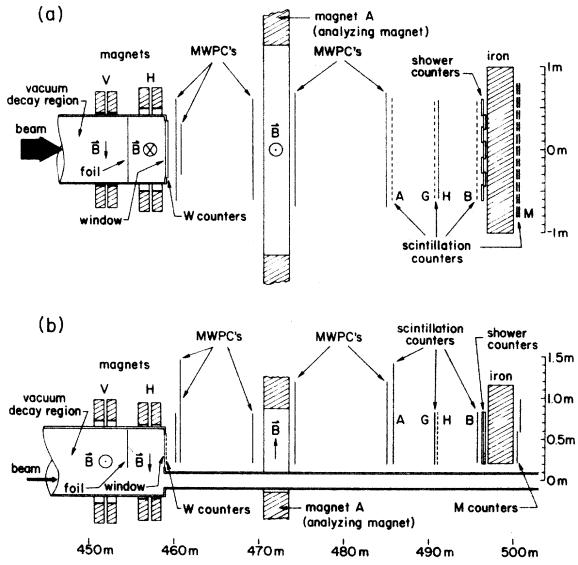

FIG. 1. (a) Plan view and (b) elevation view of the detection apparatus. Also shown in the elevation view is the vacuum system in which the neutral beam traveled. The horizontal scale is in meters from the target.

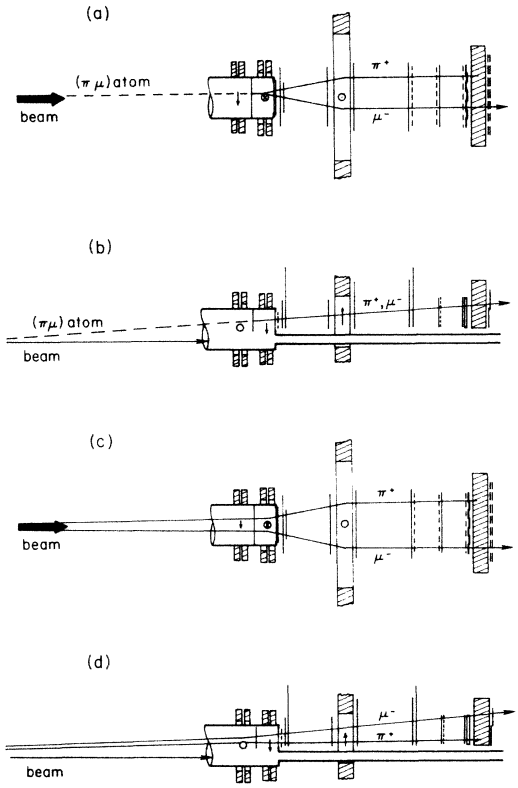

FIG. 2. Schematic illustration of differing topologies of foil and nonfoil events. (a) Plan view and (b) elevation view of a pi-mu atom which is ionized in the foil. (c) Plan view and (d) elevation view of a $K_{\mu 3}$ event, with pion and muon clearly separated.

events. It also restored the initial opening angle between tracks from nonfoil events, yielding approximately parallel trajectories. Equally spaced hits in two banks of vertical scintillation counters (A and B) identified events with approximately parallel tracks. By requiring all events to pass a parallelism requirement in the trigger, we avoided a potential difference between the foil and nonfoil triggers, while reducing somewhat the acceptance of the copious $K_{\mu 3}$ decays. Magnet V also served to lower the acceptance of $K_{\mu 3}$ decays. These effects combined to allow triggering on both atoms and $K_{\mu 3}$'s at an acceptable rate.

The experimental technique thus consisted of collecting both classes of events concurrently and then identifying pi-mu atoms and $K_{\mu 3}$'s. A Monte Carlo calculation of the relative pi-mu atom and $K_{\mu 3}$ detection efficiencies then enabled the branching ratio to be determined.

While following the procedure just described, we were also able to identify events with $\gamma \rightarrow e^+e^-$ conversions in the foil. These events came primarily from $K_L^0 \rightarrow 3\pi$ decay and were topologically similar to pi-mu atoms. Thus, the ratio of the number of observed e^+e^- pairs to the number of recorded $K_{\mu 3}$ events was related to the ratio of atoms to $K_{\mu 3}$'s and served as a monitor of the quality of the data over the course of the experiment.

B. Beam and decay region

We performed the experiment in the Meson Laboratory at Fermilab using the M3 neutral beam line, which was rebuilt in order to provide an intense K_L^0 beam. The beam was produced by 400-GeV/c protons striking a 30.5-cm-long beryllium target at targeting angles varying from 0.75 to 1.25 mr. The solid angle of the beam was defined by a hole in a 14-m-long primary steel collimator placed immediately downstream of the target and by two pairs of variable horizontal and vertical collimators located 113 and 200 m from the target. The solid angle as defined by the primary collimator was 0.9 μsr. A settling of the beam pipe at about 300 m (in an inaccessible underground area) reduced the usable solid angle to 0.1 μsr, which was reasonably compatible with the dimensions of the beam pipe underneath the spectrometer. At a distance from the target of 200 m, the maximum beam size during data taking was 5.5×1.5 in.[2] Magnets placed downstream of each pair of collimators swept aside charged particles. We inserted from 1.0 to 3.0 in. of lead in the beam at 113 m to reduce the photon component of the beam.

The principal components of this beam were neutrons and K_L^0's. The K_L^0 flux was approximately 2.4×10^7 K_L^0's per μsr per 10^{12} protons on target, which under normal data-taking conditions of 5×10^{12} protons/pulse and 6.8×10^{-2} μsr gave an intensity of about 8×10^6 K_L^0/pulse. Each pulse lasted one second. The relative fluxes of neutrons and kaons depended on the targeting angle. The n:K ratio varied from approximately 50:1 to 125:1 (Ref. 15). A typical trigger rate in the apparatus was about 250 triggers/pulse. At an accelerator repetition rate of 4 pulses per minute, we detected about one pi-mu atom every two hours. The beam intensity was limited by the singles rate that could be withstood by the spectrometer, which in turn was dominated by the neutron flux. A rate of 5×10^6 particles/pulse in the first wire chamber was maintained by varying either the solid angle of the beam or the amount of lead at 113 m.

The vacuum decay region began at 212 m and the neutral beam traveled through an uninterrupted vacuum to 535 m. At 459 m the decay region ended but the neutral beam continued, running underneath the spectrometer in a continuous vacuum to a concrete and steel dump far downstream. Particles emerging from the decay region and entering the detector passed through a thin (2.5×10^{-3} radiation lengths) vacuum window constructed primarily from a urethane-coated biaxial woven fabric.[16] This window was approximately D-shaped and filled the upper $\frac{5}{8}$ of the vacuum pipe cross section. The region from 212 to 459 m was held at a pressure of approximately 12 microns of mercury throughout the data-taking period. Neutron interactions in the residual air did not contribute to either the pi-mu atom or the $K_{\mu 3}$ signals.

The principal features of the M3 neutral beam line as used in this experiment are summarized in Table I.

C. Spectrometer magnets

We used three magnet systems in the spectrometer: magnet V, magnet H, and magnet A. Magnet V deflected particles in the vertical plane; magnets H and A deflected particles in the horizontal plane. The latter two magnets were operated with magnetic field integrals approximately equal in magnitude but with opposite polarities.

TABLE I. Properties of the Fermilab M3 neutral beam.

Target composition, length	Be, 30.5 cm
Targeting angle	0.75–1.25 mr
Solid angle	1×10^{-7} sr
Length of decay region	250 m
Volume of decay region	125 m^3
Decay region vacuum	12 microns of mercury
No. of K_L^0 per pulse and per 5×10^{12} protons	8×10^6
Proton beam momentum	400 GeV/c
Average K_L^0 momentum	65 GeV/c
Neutron/K_L^0 ratio	(50–125)/1

The main spectrometer magnet, magnet A, was used to measure the momenta of charged particles. It had an aperture 100 in. wide$\times$40 in. high$\times$40 in. along the beam and was operated with an integrated vertical field of 5.51 kG m. The three components of the magnetic field had been previously measured at a magnetic field integral of 12.6 kG m (Ref. 17). We checked this field map and determined its overall normalization by inserting a $\frac{3}{8}$-in.-thick aluminum target in the beam 400 m from the primary target and then requiring that the invariant mass of reconstructed $p\pi^-$ decays of Λ^0's produced in the aluminum target be centered on the known Λ^0 mass. The normalization was determined to 0.4% and the field map found to be adequate.

Magnet H was formed by placing two 33 in.$\times$40 in.$\times$44 in. magnets end-to-end. These magnets were normally run with a combined field integral of 5.70 kG m. The magnetic field of each magnet, including the fringe fields, had been previously measured at an integrated field of 3.36 kG m (Ref. 18). We explored this field map and determined the magnitude of the field relative to that of magnet A using single pions produced in the aluminum target at 400 m by a beam of small cross-sectional area. The momenta of these pions were measured using magnet A, and then their trajectories were tracked upstream through magnet H. By adjusting the field strength as a function of position in magnet H, the pions were made to project to the known beam location at the aluminum target. We determined the overall strength of magnet H relative to magnet A to 0.3% in this way and found that the deviations from the previously measured field map were less than 1%.

Magnet V consisted of two magnets identical to those used in magnet H. These magnets were rotated about the beam axis by 90° relative to magnet H and run at a combined field integral of 2.80 kG m. To verify the field map of magnet V, we followed the same procedure used for magnet H.

D. Ionizing foil

The aluminum foil used to ionize pi-mu atoms and convert photons was placed inside the vacuum pipe midway between magnet V and magnet H. The two different thicknesses used, 0.020 and 0.035 in., gave photon-conversion probabilities of 4.5×10^{-3} and 7.7×10^{-3}, respectively. As noted above, approximately equal amounts of data were collected with each in order to verify that all the atoms in each sample were dissociated. Each foil was D-shaped and filled the upper $\frac{5}{8}$ of the vacuum pipe cross section.

E. Counters and trigger logic

The elements of the spectrometer are shown in Fig. 1. There were six scintillation-counter banks: W, A, G, H, B, and M. The W counter bank was placed immediately after the D-shaped vacuum window and consisted of seven horizontal $\frac{1}{16}$-in.-thick counters. The active area approximated that of the window. The H bank was formed from eleven scintillators mounted horizontally and was located about 5 m downstream of the last wire chamber. The A, G, B, and M banks all consisted of vertical counters. The A, G, and B banks consisted of 22, 24, and 22 counters, respectively, and were also after the last wire chamber about 5 m apart from one another. The 22 M counters were arranged in two rows of eleven overlapping counters behind a 3-m-thick steel wall. In each bank, each counter was connected to a single photomultiplier tube. The signal from each tube was discriminated and then the signals were logically combined for each bank to determine if a specific requirement had been met, e.g., $=2A$ if two and only two A counters were struck, $\geq 2A$ if two or more were struck, etc.

A bank of shower counters was placed just before the steel wall. Each of the seven modules was made from fifteen $\frac{1}{4}$-in.-thick layers of lead, interleaved with $\frac{1}{4}$-in.-thick acrylic sheets (17.3 radiation lengths total). Adjacent counters were overlapped 1 in. The pulse from each tube was passively split into two signals. One of these was added to the signals from the other six tubes, and the resultant signal was discriminated at a level corresponding to an electromagnetic energy deposition of about 4 GeV in the bank. The other signal was integrated and digitized in an ADC and the value stored for off-line analysis. The calibration and use of these counters is described below in Sec. V B.

The pattern of hits in the A and B banks was used in selecting events of interest and reducing rates from unwanted triggers. A signal PT was formed if the pattern of struck A and B counters corresponded to two particles with approximately parallel trajectories. This signal was formed by requiring that the pattern be identical to one of a set of patterns residing in electronic memory. The electronics used to produce this signal in 190 ns has been described previously.[19]

Three different triggers were defined. The KMU3 trigger was a general trigger for two-track events with a muon. The more restrictive ATOM and E^+E^- triggers were designed to favor triggering on foil topologies over nonfoil topologies. The logic signature for $K_{\mu3}$ events was

$$\text{KMU3}\equiv(\geq 1W)\cdot(=2A)\cdot(\geq 2G)\cdot(\geq 1H)\times(2,\ 3,\ \text{or}\ 4B)\cdot(\geq 1M)\cdot\text{PT}\ .$$

(The restrictive PT requirement on the A and B banks aided in reducing the total trigger rate without biasing the pi-mu atom to $K_{\mu3}$ branching-ratio determination.) The ATOM trigger was a subclass of KMU3, defined as

$$\text{ATOM}\equiv\text{KMU3}\cdot(=1W)\cdot(=1H)\ .$$

A separate trigger for e^+e^- events was made by replacing the M-counter (muon) requirement of the ATOM trigger by the requirement that more than 4 GeV be deposited in the shower counters:

$$E^+E^-\equiv(=1W)\cdot(=2A)\cdot(\geq 2G)\cdot(=1H)\times(2,\ 3,\ \text{or}\ 4B)\cdot\text{PT}\cdot(>4\ \text{GeV})\ .$$

Under normal data-taking conditions, the KMU3 trigger was prescaled by 32. Events that satisfied any of the three triggers were recorded concurrently.

F. Wire chambers

The particles' trajectories were measured using multiwire proportional chambers (MWPC's) which had been used in previous experiments.[20] Each of the five chambers contained two orthogonal signal planes. Chambers 1, 3, and 4 (see Fig. 1) had sets of vertical and horizontal wires which measured positions in the top and side view, respectively. Chamber 2 had wires inclined at $\pm 45°$ to the vertical, whereas chamber 5 was rotated by 42 mr relative to 1, 3, and 4. Chamber 3 was split, with separate readouts for the left and right halves of the horizontal wires. The first three chambers had 24 in.$\times$48 in. active areas while chambers 4 and 5 were each 39 in.$\times$55 in. The chambers had $\frac{1}{16}$-in. anode wire spacing with a $\frac{3}{16}$-in. gap between the anode and cathode planes. The working gas was Ar-CO_2-Freon in the ratio 0.8:0.2:0.0025. The efficiencies of the chamber planes depended upon the particle flux through them and varied from about 89% to 98%. We discuss the effect of these inefficiencies in Sec. V A. Thin-walled bags filled with helium (not shown in Fig. 1) were inserted among the last four chambers to reduce multiple scattering.

G. Data acquisition

The data-acquisition system was controlled by a PDP 11/45 computer. An auxiliary memory consisting of 64$\times$1024 (64K) 16-bit words was used as an interface between the computer and the readout electronics of the proportional chambers.

The data-acquisition sequence was as follows. Whenever a trigger occurred, up to 64 words of chamber hit information were written directly into the 64K memory. Then the computer was interrupted and the data-acquisition program continued the readout. The trigger counters' hit information, which had been latched in ten 16-channel coincidence registers interfaced directly to the PDP 11 UNIBUS, was transferred to the 64K memory. Then the pulse-height information from the shower counters was deposited in the 64K memory. Pulse heights were digitized by a LeCroy 2249 10-bit ADC module that had been modified to communicate with the PDP 11/45 directly over the UNIBUS rather than through CAMAC. The entire readout sequence for one event required 250 μs, during which time no new trigger was accepted. A typical event record length was 50 words. All of the data from one beam pulse were temporarily stored in the 64K memory and then the accumulated contents were transferred to magnetic tape between beam pulses.

IV. MONTE CARLO CALCULATION

We carried out a detailed Monte Carlo simulation of the experiment in order to determine the ratio of the detection efficiencies for pi-mu atoms and $K_{\mu 3}$ decays. By comparing Monte Carlo–generated events to data, we were also able to search for and study potential sources of systematic errors. In addition, we calculated backgrounds from decays such as $K_L^0 \to \pi e \nu$ (K_{e3}) and $K_L^0 \to \pi^+\pi^-\pi^0$ ($K_{\pi 3}$) using the same Monte Carlo program.

K_L^0's were produced at the target according to an input momentum distribution and then decayed over the length of the decay volume. For each event the K_L^0 direction was chosen randomly within a beam of cross-sectional area 3 in.$\times$1 in., 4 in.$\times$1 in., 5 in.$\times$1 in., or 5.5 in.$\times$1.5 in. at 200 m. These beam solid angles corresponded to the predominant collimator settings during data taking. The input K_L^0 momentum spectrum was determined by an iterative comparison of $K_{\mu 3}$ events in the data with Monte Carlo–generated events. The starting point in this procedure was a spectrum derived from the parametrizations of the inclusive K_S^0 differential cross section obtained by Edwards *et al.*[15] and Skubic *et al.*[21] for 200- and 300-GeV/c protons incident upon a beryllium target. Figure 3 shows the final input momentum distribution.

Events from many K_L^0 decay modes were generated. Pi-mu atoms were generated isotropically in the K_L^0 rest frame with a momentum of 188 MeV/c. The atoms were tracked as neutral particles to the stripping foil where they were immediately considered ionized to their charged components which were then allowed to multiple scatter in the foil. The pion and muon energies for $K_{\mu 3}$ events were chosen according to a standard parametrization of the matrix element,[11] supplemented by the order-α virtual-photon radiative corrections calculated by Ginsberg.[13] The energies of the decay products for K_{e3} and $K_{\pi 3}$ events were also chosen according to standard expressions for the Dalitz-plot density[11] but without including radiative corrections.

Photons arising from K_L^0 decay came primarily from the decays $K_L^0 \to \pi^0\pi^0\pi^0$, $K_L^0 \to \pi^+\pi^-\pi^0$, and $K_L^0 \to \pi^0\pi^0$, each followed by $\pi^0 \to \gamma\gamma$. The decays $K_L^0 \to \gamma\gamma$ and $K_L^0 \to \pi e \nu \gamma$ were also present and simulated, the latter using the theoretical photon energy spectrum of Fearing, Fischbach, and Smith.[12] The photons were projected to the stripping foil where they were converted to e^+e^- pairs.[22] Another source of e^+e^- pairs at the foil was electron trident production by electrons from K_{e3} decay. Tridents could fake converting photons if the energy of the produced positron was large and one of the two electrons in the final state was lost. These events were simulated using calculated distributions.[23]

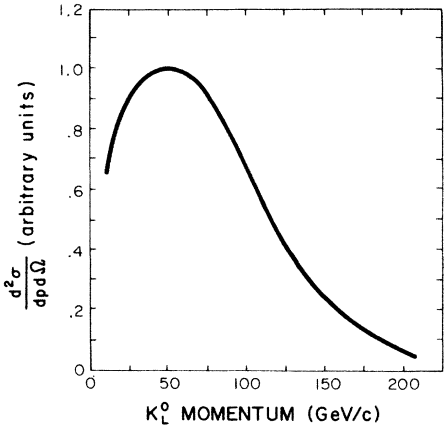

FIG. 3. Kaon momentum spectrum (at the target) used as input to the Monte Carlo calculation.

Pion and muon decays were included for all Monte Carlo events. Pi-mu-atom events were not accepted if either the pion or the muon decayed before the atom reached the foil. Otherwise, pion and muon decays were handled no differently for pi-mu-atom events than they were for other kaon-decay modes.

In generating events with an e^+e^- pair produced by a photon converted in the foil, we studied the other photons from the K_L^0 decay (up to 5 in $K_L^0 \to 3\pi^0$) to see if they interfered with the event. Showers produced by these photons were generated using the EGS program.[24] If the shower products which entered the detector caused the event to fail to satisfy the trigger, the event was rejected.

Each particle from the K_L^0 decay was tracked through the apparatus. The position of the target, the direction of the beam, the location of the beam pipe, and the location of each element of the detector were determined either by surveying or through analysis of the data itself. We estimated errors on these measurements and studied their effect on the relative acceptance. All magnetic fields were approximated by step functions which turned on at the magnets' pole pieces. Charged particles were tracked through each magnet in helical trajectories using the maps of field integrals that had been measured for each magnet.

Multiple scattering in each element of the detector was simulated using one of two techniques. For the thin elements (all but the shower counters and the steel wall), we used the normalized scattering angle distributions of Marion and Zimmerman[25] scaled by the parametrization of Highland.[26] The algorithm used to determine the angular and transverse displacement of the particles in the two thicker elements followed that of Rossi[27] and included the ionization energy loss.

Energy loss by bremsstrahlung radiation was simulated for electrons using the Bethe-Heitler[27] formula. The tail of this distribution was manifest in the slight departure of the electron and positron tracks from parallelism downstream of the analyzing magnet.

The intercepts of tracks in the MWPC planes were converted to wire hits using the following approximation. The distance between two adjacent wires was divided into three regions with the middle one equidistant from both wires. If a track passed through the central region, both wires were considered struck. A track in one of the other two regions struck just the nearest wire. The width of the middle region was determined by the observed frequency of one-wire and two-wire hit events in the data. The position resolution obtained in this manner agreed with that found in the data. In addition, the measured global efficiency of each plane was included.

Hits were also recorded for each struck counter. Counter inefficiencies caused small differences in the ratio of the total pi-mu-atom to $K_{\mu 3}$ acceptances, due to slightly different illuminations. Therefore, the efficiencies of all counters were included in the Monte Carlo calculation. Also, each track could have associated with it extra hits from δ rays. The probability and pattern of these extra hits were determined using single muons collected with a steel beam stop inserted in the neutral beam.

Monte Carlo events were required to satisfy the same trigger requirements as the raw data, and then both Monte Carlo and data events were processed by the same analysis programs.

V. DATA ANALYSIS

A. Track-finding method

Ten MWPC planes, with an average efficiency of 94%, were used to measure positions along the tracks. Two different, complementary, track-finding algorithms were developed. The goal of the first track-finding method was to maximize the number of pi-mu-atom events identified without compromising our understanding of the relative retrieval efficiency for atom and $K_{\mu 3}$ events. The goal of the second track-finding method was strictly to maximize the number of pi-mu atoms which could be retrieved from the raw data. The differences between the two stemmed from the fact that the side-view projections of the two pi-mu-atom tracks lay virtually on top of one another, whereas, due to magnet V, $K_{\mu 3}$ events always had two separated tracks when viewed from the side. Events in which only one side-view track was found were considered good pi-mu-atom candidates and that one side-view track was assigned to both top-view tracks. Atomlike events were thus inherently easier to retrieve than $K_{\mu 3}$ events because only one of the two side-view tracks needed to be identified. Furthermore, since the two side-view tracks of atomlike events were virtually identical, it was unnecessary to make an unambiguous correlation between the top and side-view tracks. For $K_{\mu 3}$ events, however, it was necessary to utilize the information in the two rotated chambers in order to correlate the two top and two side-view tracks. Again, this made it relatively simpler to retrieve pi-mu-atom events.

The first track-finding method purposely did not take full advantage of these simple atom features when their effect on retrieval efficiency was difficult to calibrate in the presence of inefficient chambers. However, the first method did succeed in finding a sample of atoms which could be used to make a reliable measurement of the ratio R [Eq. (1)]. The procedure was as follows. Any side-view track segment was allowed to be missing a hit in any one of chambers 1, 2, 3, or 4. Since chamber 5 had been rotated by 42 mr, the two tracks in a foil event could be differentiated in this chamber, allowing the hit requirements here to be the same for both classes. In addition, the orthogonal projections of at least one of the tracks were required to be correlated using chamber 2 (which had wires rotated by 45°). This technique reduced the sensitivity of the ratio of the retrieval efficiencies for the two classes to the chambers' efficiencies. Using the measured efficiencies, the foil to nonfoil event retrieval ratio was found to be 1.024 ± 0.027, normalized to the relative retrieval efficiency for perfectly efficient chambers. The error on this ratio includes a contribution from possible biases in the track-finding algorithm itself, as well as a contribution from the errors on the measurements of individual chamber efficiencies.

The second track-finding algorithm took full advantage of all the topological features of pi-mu atoms (two tracks emerging from a vertex in the center of magnet H in the

top view, parallel after magnet A in the top view, nearly coincident in the side view, etc.). As a result, less information was needed from the two rotated chambers, and the adverse effects of chamber noise and inefficiencies were minimized. This method succeeded in finding 65% more pi-mu atoms than the first. These were used to study shapes of kinematic distributions (transverse momentum, lifetime, etc.), where an absolute normalization was not necessary. A large sample of e^+e^- events was also retrieved, due to their topological similarity to pi-mu atoms. These e^+e^- events were used to verify that the shapes of kinematic distributions were independent of the track-finding algorithm. A simple version of the second method was also implemented on line in PDP 11 assembly language, so that e^+e^- events could be displayed and monitored during data acquisition.

In the following discussion, all quantities and figures relevant to the measurement of the branching ratio R were obtained using the first track-finding method.

B. Particle identification

Leptons were identified using the lead-Lucite shower counters and the M hodoscope which followed a 3-m-thick steel wall. Hadrons could be identified only by the absence of a lepton signal. The shower counters were tuned and studied using well-identified e^+e^- pairs and K_{e3} events.

A quantity called F_n (where n was 1 or 2 for two-track events) was defined as the fraction of the nth particle's energy (as measured by the magnetic spectrometer) which was deposited in the shower counter it struck. An electron typically deposited about 98% of its energy in the shower counters. Figure 4 gives the F_n distribution for electrons from photon conversions. For particles incident on the overlapped regions of the shower counters, F_n was determined by summing F_n for the two overlapped counters. For about 5% of the events, both tracks projected to the same counter, in which case F_n could not be determined separately for each particle. A different quantity F_{total} was then defined to be the ratio of the total energy deposited in the shower-counter bank to the sum of the two charged momenta.

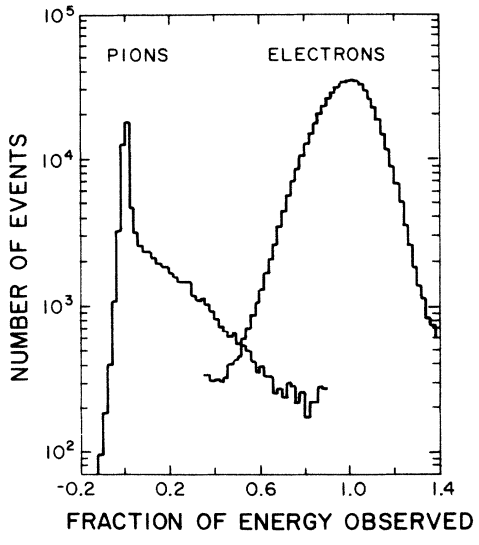

FIG. 4. The quantity F_n, defined as the energy in the struck shower counter divided by the momentum of the particle as measured by the magnetic spectrometer.

Kinematically identified K_{e3} events were used to determine the F_n distribution for pions (pions had about a 40% probability of interacting in the shower counters). If the F_n of one of the particles from these events was greater than 0.85, it was identified as an electron and the other particle was called a pion. Figure 4 also shows the F_n distribution for these pions.

In selecting π-μ events (pi-mu atoms and $K_{\mu 3}$'s), either both particles were required to have F_n less than 0.7 with one less than 0.2, or F_{total} was required to be less than 0.6. Electron-positron pairs were required to have either both F_n's greater than 0.7 or F_{total} greater than 0.7. From the distributions in Fig. 4 we determined that 96% of the pions and 2.7% of the electrons had F_n below 0.7.

Though the F_n requirements for π-μ events just described were used to select a muon ($F_n < 0.2$) and a pion ($F_n < 0.7$), the shower counters were not used to determine which particle was the muon. That was accomplished using the M hodoscope information. First, the probability that a particle had scattered into the area of a struck counter was calculated assuming a Gaussian shape for the probability of displacement by a radial distance from a straight line trajectory at the hodoscope. Then, for two-track events, the particle with the highest probability was labeled the muon. If instead the muon had been identified simply as the track which projected closest to a struck M counter, then greater than 98% of the events would have had identical muon assignments following either procedure, thus demonstrating that muon identification was not sensitive to the labeling technique. In order that the muon identification be unambiguous for π-μ candidates, events were rejected if two or more nonoverlapping M counters were struck, or if the projections of the two particle trajectories at the M hodoscope were separated (in the plan view) by less than one M counter width.

As the respective final-state particles for pi-mu atoms and $K_{\mu 3}$ events had similar momentum distributions and counter bank illuminations, systematic errors in particle identification were presumed to cancel in determining the branching ratio R.

C. Event selection

There were 43×10^6 events written to tape during this experiment. 6.7×10^6 two-track events remained after track reconstruction. Of these, 4.2×10^6 were ATOM triggers, 3×10^5 were KMU3 triggers, and 2.2×10^6 were E^+E^- triggers. These events were divided into the two classes, foil and nonfoil, described in Sec. III A above (and shown in Fig. 2). The nonfoil type consisted of $K_{\mu 3}$, K_{e3}, and $K_{\pi 3}$ events. The foil type included neutral particles, namely, pi-mu atoms and photons, which ionized or converted to two charged particles in the aluminum foil. In this section, further attention is drawn to the topological

and kinematic differences between foil and nonfoil events which facilitated their clean separation.

In a foil event, the reconstructed tracks satisfied three different geometrical requirements. The two tracks were required to converge in the plan view to a point (vertex) near the midplane of magnet H, to coincide in the side view, and to be parallel downstream of magnet A. Taken together, these requirements selected events in which two charged particles followed identical trajectories immediately downstream of the aluminum foil.

The study of the convergence near the midplane of magnet H was begun by extrapolating the two tracks in three dimensions without bending from the first three chambers into the vacuum decay region. A vertex of the two tracks was defined to be the midpoint of the line segment joining the two extrapolated tracks at their closest approach to one another. The longitudinal position of the vertex is shown for raw ATOM, KMU3, and E^+E^- triggers in Fig. 5. The vertex for foil-event candidates was required to lie within 21 cm of the center of magnet, which corresponds to the peak of the distribution; the vertex for nonfoil-event candidates was required to be greater than 14 cm from the center. Figure 6 shows the separation in space of the two tracks at the vertex for the E^+E^- triggers. The tracks for foil events were required to have a distance of closest approach less than 6 mm.

In foil-event candidates for which more than one side-view track was found, the tracks were required to nearly coincide. The maximum side-view vertical separation achieved by the two tracks between chambers 1 and 5 is shown in Fig. 7 for raw triggers. The tracks of foil events were required to have a maximum vertical separation less than 3.4 cm. In addition, the two tracks had to come at least as close as 4.8 mm somewhere between chambers 1 and 5. The tracks of nonfoil events were required to achieve a maximum side-view separation greater than 1.3 cm.

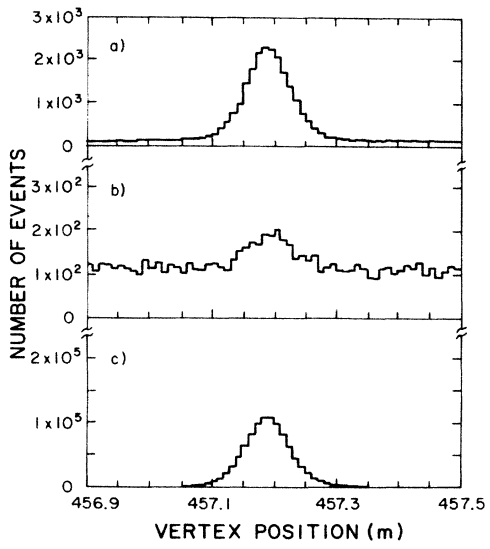

FIG. 5. Longitudinal position of the vertex of the two tracks when projected without bending through magnets V and H, for (a) ATOM, (b) KMU3, and (c) E^+E^- triggers.

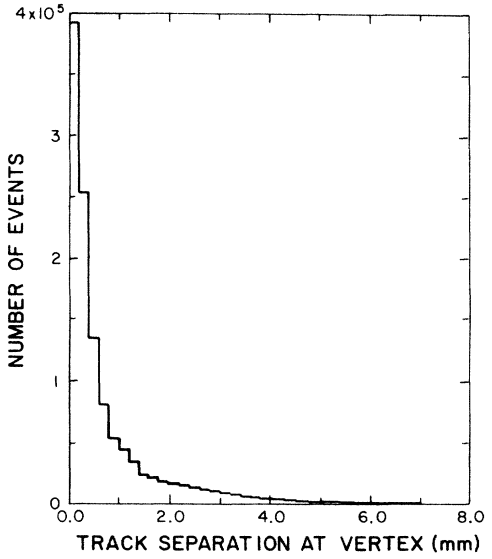

FIG. 6. Distance of closest approach of the extrapolation of the two reconstructed tracks for foil events.

The deviation of the two tracks from parallelism in the plan view downstream of magnet A is shown in Fig. 8. The quantity histogrammed is the track separation at chamber 4 minus the track separation at chamber 5, normalized to the separation at chamber 4. The peak at zero difference contains foil events, the tracks of which were parallel. The magnitude of the change in track separation of foil events was required to be less than 16%. The smaller peak to the left contains valid $K_{\mu 3}$ events, the tracks of which were slightly diverging since their original angles were restored after magnet A. No parallelism re-

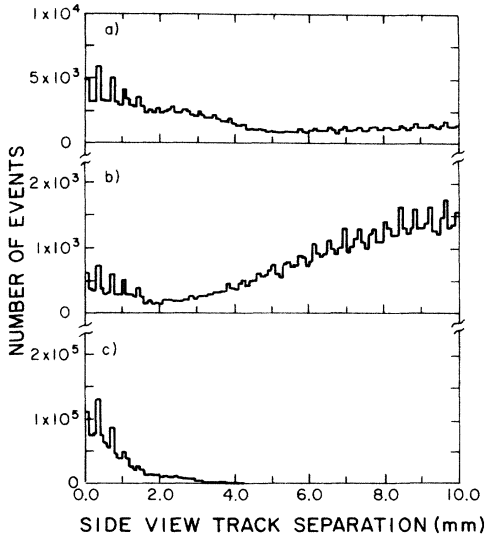

FIG. 7. The maximum side-view separation of the two reconstructed tracks, for (a) ATOM, (b) KMU3, and (c) E^+E^- triggers. Contamination by $K_{\mu 3}$ events is apparent in (a), while a small contamination by e^+e^- pairs is apparent in (b).

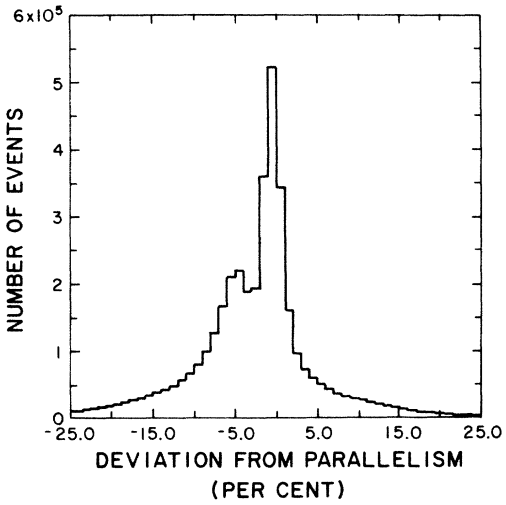

FIG. 8. The track separation at chamber 4 minus the separation at chamber 5, expressed as a percentage of the track separation at chamber 4, for both foil and nonfoil events. Foil events are peaked at zero.

quirement was imposed on these nonfoil events, other than the crude requirement imposed by the trigger logic.

Two techniques were used in tracking particles through magnet H and magnet V to determine the K_L^0 decay point. The technique depended upon the event type. For foil events, the two particles were tracked through magnet H only and then combined to determine the momentum and trajectory of the neutral parent from which it was assumed they originated. Magnet V would have had no effect upon this trajectory. The intersection of this parent particle trajectory with the pyramid of the beam was then determined, with the position of the assumed decay point located midway between the point where the line entered the beam and where it exited. The reconstructed parent trajectory of some foil events did not intersect the beam. This was noted and an alternate decay point found by determining the position of closest approach between the line of the parent particle and the center line of the beam. A foil event was accepted if either the horizontal coordinate of the decay point fell within the beam profile or the line of the parent particle trajectory intersected the beam. The reconstructed decay point was also required to be in the vacuum region between 240 and 440 m from the target.

Particles from nonfoil events were tracked through both magnet H and magnet V. A decay point was then determined from the point of closest approach. A quantity δ, defined as the distance of closest approach divided by the distance of the decay point from MWPC plane 1, served as a useful measure of the quality of the decay vertex. A nonfoil event was rejected if its decay vertex location was outside the beam or if δ was greater than 0.0015. Furthermore, nonfoil events were accepted only if the vertex was between 250 and 430 m from the target.

With the decay vertex location known, all necessary kinematic quantities could be calculated for both event classes. The transverse momentum p_T was calculated from

$$p_T=[p^2-(\mathbf{p}\cdot\hat{\mathbf{n}})^2]^{1/2}, \tag{9}$$

where $\mathbf{p}=\mathbf{p}_\pi+\mathbf{p}_\mu$ was the pair momentum and $\hat{\mathbf{n}}$ was the reconstructed K_L^0 direction (determined by the ray from the target to the reconstructed vertex). Because the neutrino went undetected, there was a twofold ambiguity in determining the magnitude of the K_L^0 momentum for π-μ events. The two solutions and a quantity Δ were calculated according to

$$p_\pm=(1\pm\sqrt{\Delta})\frac{(\mathbf{p}\cdot\hat{\mathbf{n}})X}{2[E^2-(\mathbf{p}\cdot\hat{\mathbf{n}})^2]} \tag{10}$$

and

$$\Delta=1-\frac{[(\mathbf{p}\cdot\hat{\mathbf{n}})^2-E^2](X^2-4E^2m_K{}^2)}{(\mathbf{p}\cdot\hat{\mathbf{n}})^2X^2}, \tag{11}$$

where $E=E_\pi+E_\mu$ was the energy of the pair and we defined $X=m_K{}^2-p^2+E^2$. The K_L^0 momentum was taken to be the average of the two solutions.

1. *Pi-mu atoms*

Pi-mu atoms were isolated by looking at events with the following characteristics: (a) ATOM trigger, (b) two particles of opposite charge, (c) foil-event topology, (d) unambiguous muon identification, and (e) π-μ signature in the shower counters.

The shower-counter cut (e) was imposed as described in Sec. V B above. As a further illustration, we show in Fig. 9 a histogram of F_{total} for events that satisfied cuts (a)—(d). A clear separation between a dominant e^+e^-

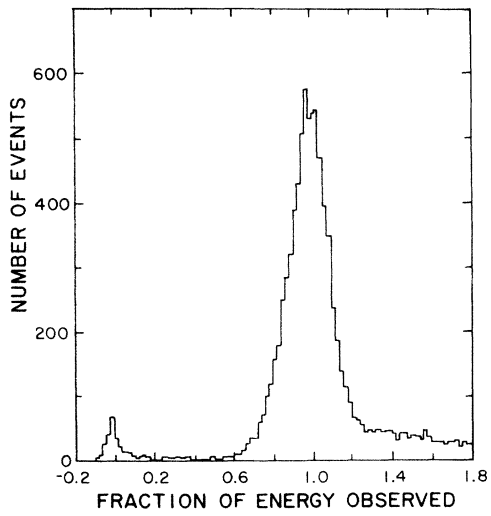

FIG. 9. The quantity F_{total}, the fraction of the event's momentum which appears as energy deposited in the shower counters, for pi-mu-atom candidates. The large peak at 1.0 was due to e^+e^- pairs with an accidental muon; these events were subsequently rejected.

signal (seen in the peak around 1.0) and π-μ events is apparent. These e^+e^- events were due to normal photon conversions with a random M counter struck.

A remaining source of background was $K_{\mu 3}$ events in which, due to inefficiencies in the side-view wire planes, only one side-view track was found. Evidence for a second track could be seen in most of these events. This background was simulated by taking $K_{\mu 3}$ events from the data and disregarding one of the side-view tracks. Because of the missing side-view track, the event was mistaken for a foil event; the effect of magnet V was thus not properly taken into account. As a result, these background events had decay vertex characteristics and kinematic distributions different from those of atoms. Curve A in Fig. 10 shows the p_T distribution for atom candidates which passed the shower-counter cuts. Curve B is the simulated background, the shape of which is evident in the excess events at higher and lower p_T in Curve A. The events at high p_T were rejected outright by requiring that atoms have a transverse momentum less than the kinematically allowed maximum, allowing for finite resolution. The background at low p_T was controlled by the subsequent requirement that the atom extrapolate back to the beam. Thus, the last two cuts were the following: (f) $p_T < 210$ MeV/c, and (g) good K_L^0 decay vertex.

We now introduce a dimensionless quantity α, defined by

$$\alpha = \frac{(p_\pi - p_\mu)}{(p_\pi + p_\mu)} . \tag{12}$$

For dissociated atoms, the pion and muon have nearly the same velocity, and hence α should be the difference over the sum of the pion and muon masses, equal to 0.14. Figure 11 shows the distribution of α after all requirements were imposed; a clear pi-mu-atom signal is centered at 0.14. There is another peak at -0.14 containing 0.015 times as many events as seen at $+0.14$. These are valid pi-mu-atom events for which the pion and muon assignments were reversed. This ratio was consistent with the Monte Carlo simulation, as was the width of the peaks (determined by the momentum resolution of the spectrometer).

The remnant pi-mu-atom background outside the peaks has the shape predicted by the simulation described above of $K_{\mu 3}$ events with a missing side-view track. A background subtraction using this shape to extrapolate underneath the peaks left an atom signal of 154.8 events in the range $0.08 < \alpha < 0.20$ above a background of 8.2 ± 2.1 events. Of these 163 candidates, 90 were $\pi^+\mu^-$ and 73 were $\pi^-\mu^+$.

By using the second track-finding method (Sec. V A) and relaxing other requirements relevant only to absolute normalization, we could enlarge the sample of pi-mu-atom candidates. The histogram of α for this larger sample is shown in Fig. 12, where 320 signal events are in the peak above a background of 35 ± 7 events. Starting from the sample of 163 events, an additional 123 events were obtained by relaxing the track-finding requirements. Allowing events which passed outside of the active area of

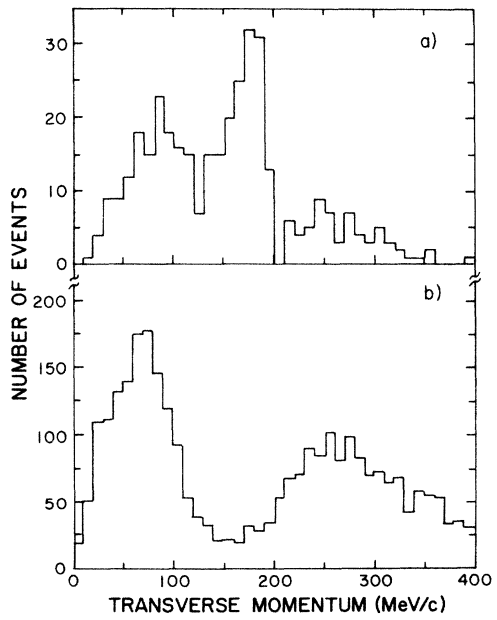

FIG. 10. Transverse momentum of events passing previous pi-mu-atom cuts: (a) real atom data and (b) background shape simulated by removing one side-view track from real $K_{\mu 3}$ events and processing them as if they were ATOM triggers.

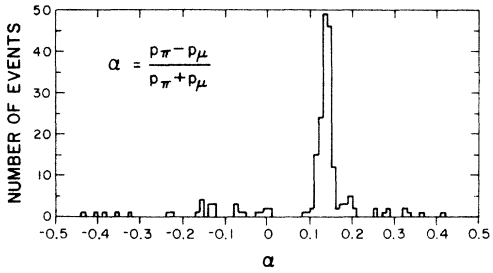

FIG. 11. Histogram of the variable α after all cuts, for atoms retrieved by the first track-finding method.

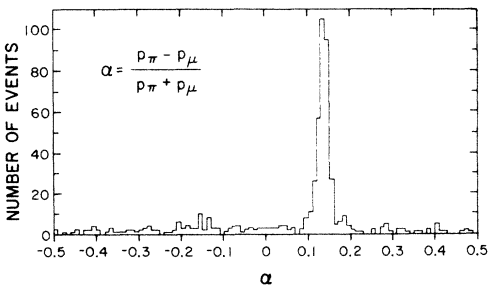

FIG. 12. Histogram of the variable α after all cuts, for atoms retrieved by the second track-finding method, with some cuts relaxed.

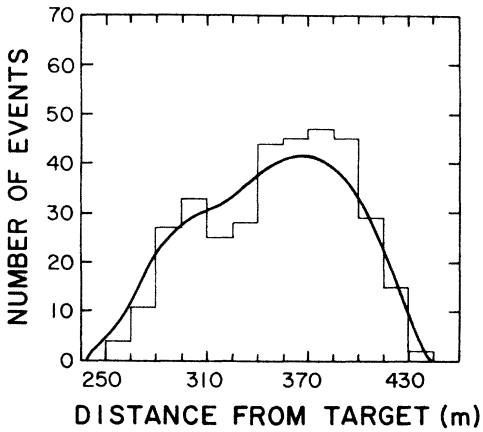

FIG. 13. Data and Monte Carlo prediction for the reconstructed longitudinal position of the decay $K_L^0 \rightarrow$pi-mu atom $+\nu$.

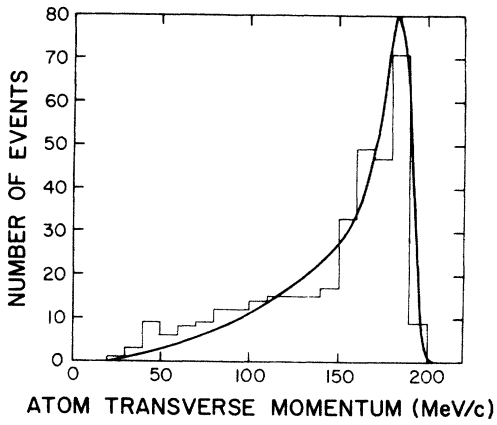

FIG. 15. Data and Monte Carlo prediction for the transverse momentum of pi-mu atoms.

various wire planes (primarily MWPC 2, see Fig. 1) gave 44 additional events. Finally, 25 pi-mu atoms were collected during runs with nonstandard KMU3 triggers (but with the normal ATOM trigger).

Figures 13—16 are histograms of quantities associated with the atoms in the larger sample, with the Monte Carlo predictions superimposed. Figure 13 shows the distribution in the longitudinal position of the reconstructed kaon-decay point. Figure 14 shows the laboratory momentum. Figure 15 shows the component of momentum transverse to the reconstructed kaon's direction. The Jacobian peak in the data is in excellent agreement with the Monte Carlo prediction. Finally, Fig. 16 shows the distribution in proper time from creation to ionization, i.e., the reconstructed time, in the pi-mu-atom's rest frame, that the atom spent traveling from the kaon-decay point to the aluminum foil. All of the data distributions are statistically indistinguishable from the Monte Carlo distributions.

2. $K_{\mu 3}$'s

$K_{\mu 3}$'s were required to have the following characteristics: (a) KMU3 trigger; (b) two particles of opposite charge; (c) nonfoil-event topology; (d) unambiguous muon identification; (e) π-μ signature in the shower counters; (f) 90 MeV/c $< p_T <$ 195 MeV/c; (g) good K_L^0 decay vertex. In addition, we followed previous experimenters[28] in defining a quantity $p_0'^2$ by

$$p_0'^2 = \frac{(m_K{}^2 - m_\pm{}^2 - m_{\pi^0}{}^2)^2 - 4(m_\pm{}^2 m_{\pi^0}{}^2 + m_K{}^2 p_T{}^2)}{4(p_T{}^2 + m_\pm{}^2)}, \quad (13)$$

where $m_\pm$ represents the invariant mass of the two charged particles assuming both were pions. This quantity, when computed assuming a $K_{\pi 3}$ decay, is positive for $K_{\pi 3}$ events and negative for $K_{\mu 3}$ events, in the absence of

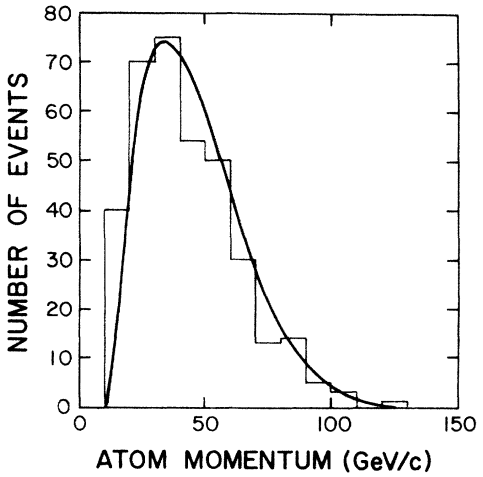

FIG. 14. Data and Monte Carlo prediction for the laboratory momentum of pi-mu atoms.

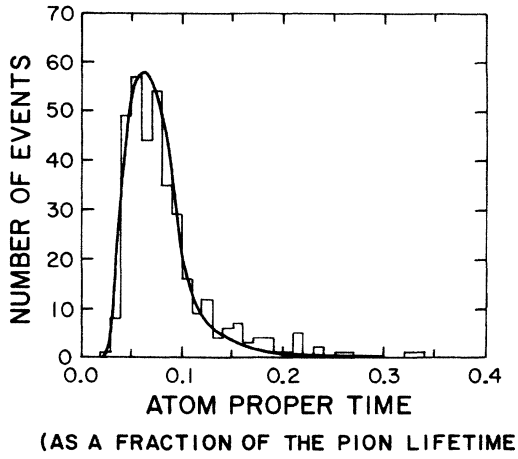

FIG. 16. Data and Monte Carlo prediction for the elapsed time, in the pi-mu-atom's rest frame, from the kaon decay to ionization in the foil, expressed as a fraction of the charged-pion lifetime.

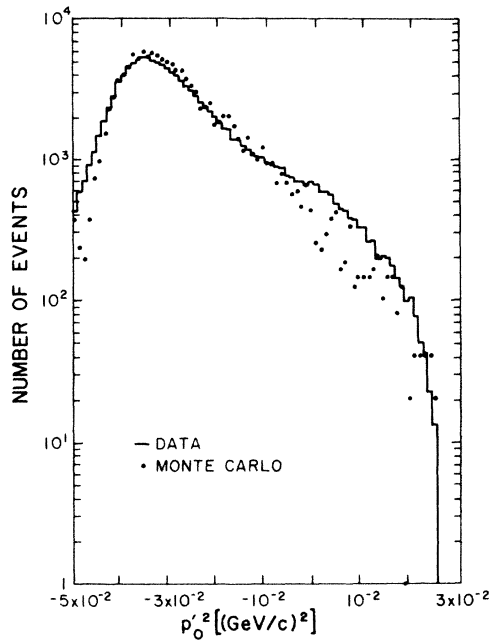

FIG. 17. Data and Monte Carlo prediction for the kinematic variable $p_0'^2$ [defined in Eq. (13)] for $K_{\mu 3}$ events, after all other cuts.

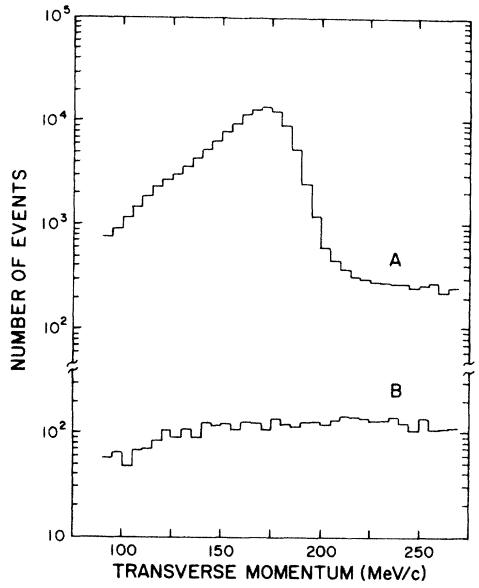

FIG. 18. The transverse momentum of unbound pi-mu events after decay vertex cuts. Events in which the pion and muon had opposite charges are shown in curve A; those with like charge are shown in curve B.

measurement errors. A histogram of $p_0'^2$ for $K_{\mu 3}$ candidates passing all of the above cuts is shown in Fig 17. We required that $p_0'^2$ be between -0.047 (GeV/c)^2 and 0.002 (GeV/c)^2 and thereby eliminated some residual $K_{\pi 3}$ and K_{e3} events.

There were two broad classes of remaining background to $K_{\mu 3}$ events. The first came from single K_L^0 decays, such as $K_{\pi 3}$ and K_{e3}, with a subsequent pion decay. About 20% of these pions decayed before they reached the shower counters. The size of this background was calculated by Monte Carlo technique using the known branching ratios for these decay modes. This calculation gave a background contribution of 0.76% from $K_{\pi 3}$'s and, assuming 2.7% of e-μ events were misidentified as π-μ events, 0.07% from K_{e3}'s.

The second class of $K_{\mu 3}$ background arose either from different K_L^0 decays producing two randomly coincident tracks or from neutrons and K_L^0 decay products in the beam halo that interacted with the beam pipe producing two-track events. Neither source was a single K_L^0 decay; the two sources were collectively called "nonbeam" background. We devised four methods of estimating the nonbeam background contribution. Their average was then used.

The first method simulated the nonbeam background by combining two particles from separate KMU3 trigger events. A variety of distributions for those simulated events which had particles of like charge agreed with the corresponding distributions in the real like-charge data. (Real like-charge data were overwhelmingly from sources other than events with a single kaon decay.) The $K_{\mu 3}$ background was then determined using the simulated opposite-charge events.

The other three background estimation methods made use of the p_T distributions for opposite-charge and like-charge events following K_L^0 decay vertex requirements, shown in Fig. 18. The $K_{\mu 3}$ events (curve A) have a kinematic cutoff at about 195 MeV/c whereas the events with same-sign charge (curve B) are distributed uniformly through this region. The distribution in any variable for opposite-charge nonbeam background events with p_T between 195 and 250 MeV/c should be similar to those whose p_T is less than 195 MeV/c. Studies of like-charge events confirmed this expectation. Accordingly, methods 2–4 each used a distribution of a different variable to estimate the total nonbeam background. Those used were the p_T itself, the horizontal distance of the kaon-decay vertex from the beam center, and the longitudinal position of the vertex. In each of these distributions a region existed which was dominated by background events. We es-

TABLE II. Sources of $K_{\mu 3}$ background.

Source	Contribution (%)
A. $K_L^0 \to \pi^+\pi^-\pi^0$ followed by $\pi \to \mu\nu$	0.76±0.10
B. $K_L^0 \to \pi e\nu$ followed by $\pi \to \mu\nu$	0.07±0.04
C. Nonbeam background	
Method 1: 7.40±0.35	
Method 2: 4.39±0.17	
Method 3: 3.86±0.16	
Method 4: 3.88±0.53	
Average nonbeam background	4.41±0.57
Total $K_{\mu 3}$ background	5.24±0.58

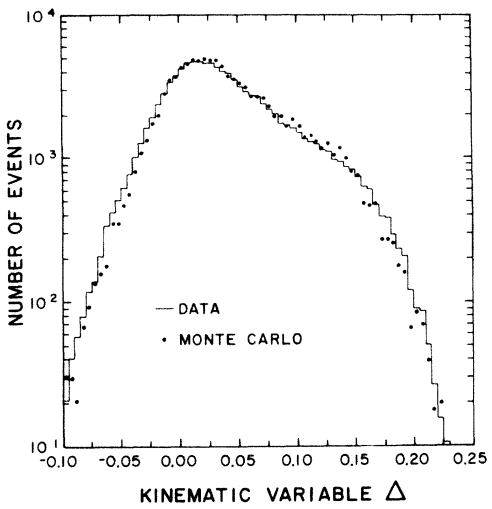

FIG. 19. Data and Monte Carlo prediction for the kinematic variable Δ [defined in Eq. (11)] for $K_{\mu 3}$ events.

timated the total number of background events using the higher-p_T events in these regions.

The average of these four techniques gave a nonbeam background contribution of $(4.41\pm0.57)\%$ where the error has been scaled by a factor of $(\chi^2/\mathrm{DF})^{1/2}$. This gave a total $K_{\mu 3}$ background of $(5.24\pm0.58)\%$. A summary of all $K_{\mu 3}$ background sources is given in Table II.

We now describe some of the ways in which $K_{\mu 3}$ events were used to study various properties of the apparatus and to confirm the Monte Carlo calculation. The Δ distribution, defined by Eq. (11), is shown in Fig. 19 for $K_{\mu 3}$ data and Monte Carlo events. This parameter is extremely sensitive to measurement and calibration errors. Of particular interest is the fraction of events with $|\Delta| < 0.01$ (referred to as "unambiguous" events: those whose two K_L^0 momentum solutions differed from their average by less than 10%). In Fig. 20, this fraction is plotted for Monte Carlo events in which the K_L^0 production target's vertical position used in the reconstruction program differed from that used to generate the events. The sensitivity of this parameter to the target position allowed us to determine the target position to about 1 cm using the reconstruction program. As the target was 450 m from the apparatus, this gave a sensitivity of about 20 μrad on the K_L^0 beam direction. Figure 20 also shows the target sweep for the data, from which the actual target position was determined.

Another parameter sensitive to the measurement of the particles' trajectories was the quality of the $K_{\mu 3}$ vertex as measured by δ, the suitably scaled distance of closest approach defined previously. Agreement between plots of δ for data and Monte Carlo events is evident in Fig. 21, demonstrating that the requirement that the δ be less than 0.0015 had the same effect on both the data and Monte Carlo events.

Figure 22 shows the data versus Monte Carlo comparison for the longitudinal decay vertex distribution. A slight excess of Monte Carlo events is seen in the far upstream region. We could have removed this excess by varying the location of the pipe at 321 m within its measurement error in the Monte Carlo calculation. Instead, the Monte Carlo program used the pipe's surveyed location; the effect of the disagreement was included in the systematic errors. This and other uncertainties in the

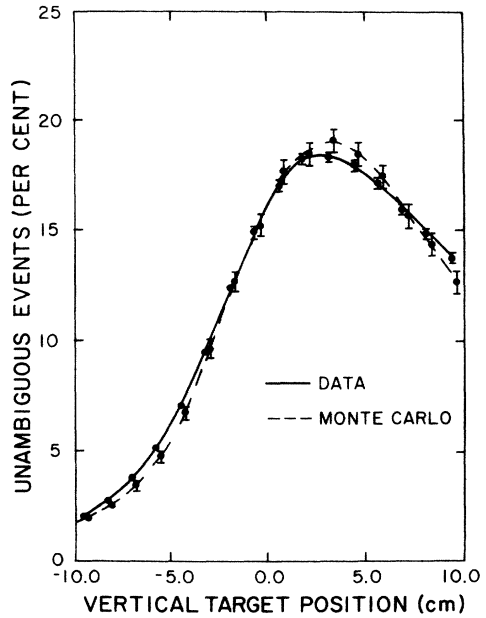

FIG. 20. Fraction of $K_{\mu 3}$ events for which the reconstructed K_L^0 momentum was unambiguous, i.e., the two solutions in Eq. (10) were within 10% of their average ($|\Delta| < 0.01$). The fraction is plotted as a function of the target position assumed by the reconstruction program. The curves are hand drawn to guide the eye.

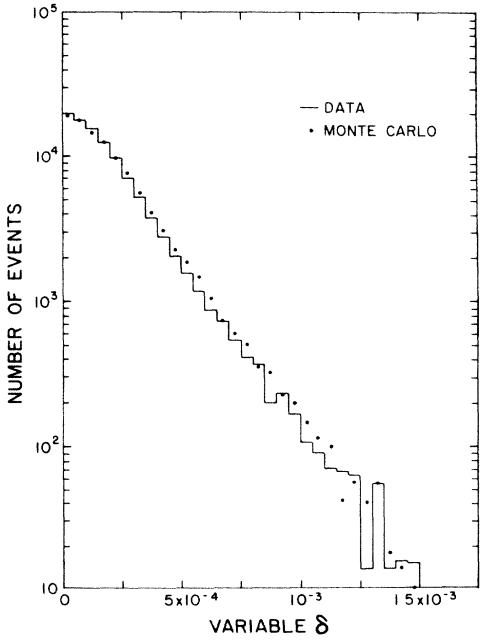

FIG. 21. Data and Monte Carlo prediction for the variable δ (defined in the text) that measures the quality of the kaon-decay vertex for $K_{\mu 3}$ events.

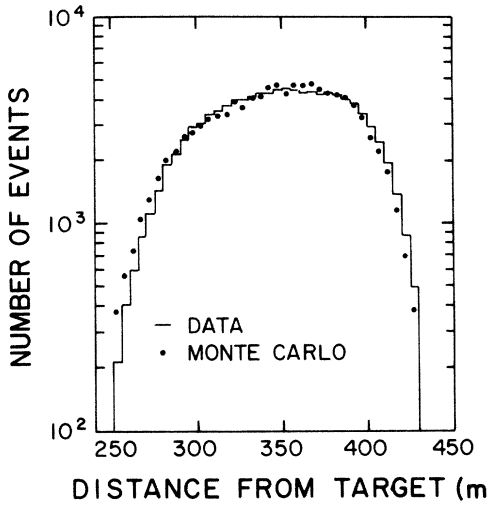

FIG. 22. Data and Monte Carlo prediction for the reconstructed longitudinal position of $K_{\mu 3}$ decays.

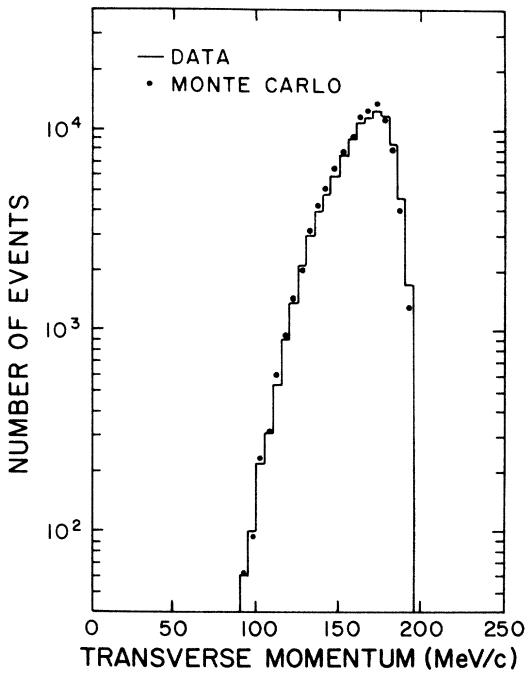

FIG. 24. Reconstructed sum of the transverse momenta of the pion and muon in $K_{\mu 3}$ events, showing data compared with the Monte Carlo simulation.

Monte Carlo calculation are discussed in Sec. VII.

For completeness, we show in Fig. 23 the histogram of the reconstructed laboratory momentum of the parent kaon [the average of the two solutions in Eq. (10)]. The input momentum spectrum (Fig. 3) was tuned within errors in order to minimize the disagreement between the data and the Monte Carlo prediction. We plot the transverse momentum of the unbound pi-mu system relative to the kaon direction in Fig. 24.

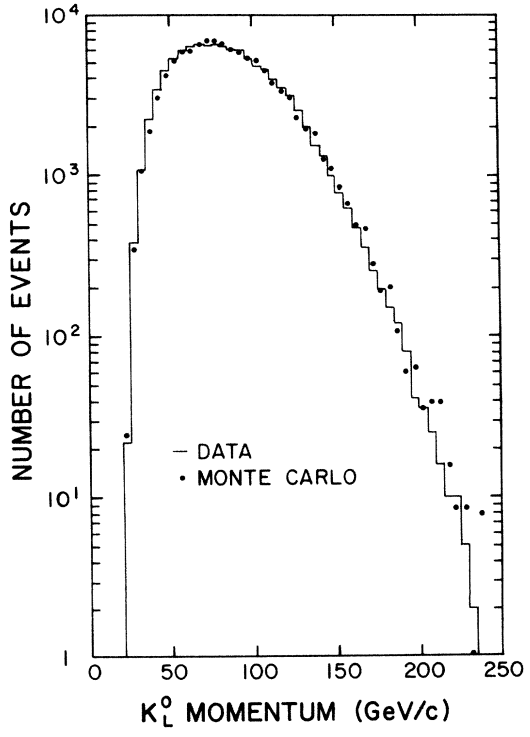

FIG. 23. Reconstructed K_L^0 laboratory momentum for $K_{\mu 3}$ events, showing data compared with the Monte Carlo simulation

3. *Electron-positron pairs*

Electron-positron (e^+e^-) pairs were selected by the following requirements: (a) E^+E^- trigger; (b) two particles of opposite charge; (c) foil-event topology; (d) e-e signature in the shower counters; (e) good K_L^0 decay vertex.

While not used directly to measure the rate of production of pi-mu atoms, e^+e^- pairs were extremely useful for enhancing and verifying our understanding of the detector performance and the data analysis programs. As emphasized earlier, e^+e^- pairs from photons which converted in the aluminum foil had topologies similar to pi-mu-atom events. The analysis of these events is described in detail in Ref. 7. We limit ourselves here to a discussion of the distribution of the component of momentum of the reconstructed photon transverse to the kaon direction (as determined from the known target position and the reconstructed kaon-decay vertex). This p_T spectrum for single photons contained components from various K_L^0 decays, as well as two known sources of background: neutral pions made in interactions of the neutral beam with residual gas in the decay region, and tridents created by electrons hitting the aluminum foil. The shape of the beam-gas background was measured by taking data with the vacuum spoiled so that these events dominated kaon de-

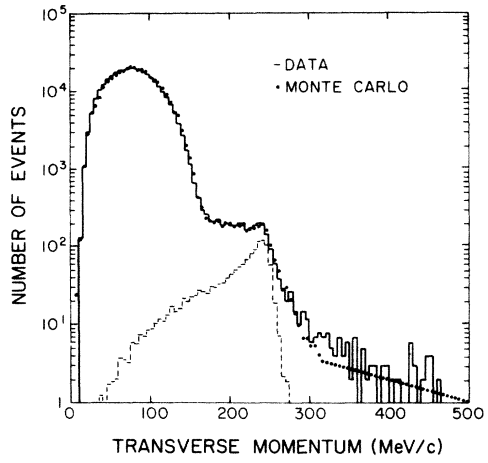

FIG. 25. Transverse-momentum spectrum of reconstructed single photons, showing data (solid line), full Monte Carlo prediction after fit (dots), and Monte Carlo prediction for the component due to $K_L^0 \to \gamma\gamma$ (dashed line).

cays. The trident background was simulated as described above (Sec. IV) with the aid of distributions of the fraction of the pair's momentum which was carried by the electron. A fit to a sum of the Monte Carlo predictions for the shapes of the various components of the spectrum was made. All of the shapes were fixed, and only the relative scales of the various components were allowed to vary. The results of the fit were consistent with known branching ratios.

Figure 25 shows the p_T distribution for the data and the result of the fitted simulated data. The large peak at low p_T is due to three-pion decays of the K_L^0. Two-pion decays yield photons of intermediate p_T. Of particular interest is the two-body decay $K_L^0 \to \gamma\gamma$, for which there is a Jacobian peak similar to that seen for atoms in Fig. 15. The events beyond the sharp cutoff of this component are background from tridents and beam-gas interactions. The agreement between the data and simulation over several orders of magnitude demonstrates our understanding of the response of the spectrometer to events with the foil topology.

VI. TRIGGER CORRECTIONS

As described in detail in Sec. III E, the ATOM trigger was a subclass of the KMU3 trigger and required one and only one struck counter in each of the two banks of horizontal counters (W and H). In order to measure the pi-mu-atom rate of formation, it was necessary to know the number of atom events which failed this trigger because more than one counter was hit in either of these banks. More than one H or W counter could be hit in a pi-mu-atom event either because the pion and muon trajectories deviated in the side view due to multiple scattering or because there were additional particles in the event. Multiple scattering caused 4.5% of the pi-mu atoms to fail the trigger requirement, according to Monte Carlo calculations.

There were two sources of additional particles: δ rays produced by the pion or muon, and random particles from other K_L^0 decays or neutron interactions. The δ ray contribution was measured using the single-muon data set; the probability of observing such an extra track was 1.1% in the W bank and 2.5% in the H bank. The effect of δ rays was incorporated into the Monte Carlo generation of pi-mu-atom and $K_{\mu 3}$ events using these results.

The probability that an extra counter was struck by a random track was found by comparing the number of hits in the two banks in $K_{\mu 3}$ events to that of Monte Carlo events (which included multiple scattering and δ rays) and assuming the excess in the data was due to random tracks. This gave an extra-hit probability due to random tracks of $(6.8 \pm 1.0)\%$. Since the Monte Carlo program included the first two causes of extra hits, this error represents the systematic uncertainty on the percentage of pi-mu-atom events which did not satisfy the trigger due to all causes.

Figure 26 shows the probability of an extra hit versus the singles rate in the W bank. The probability increases linearly with the singles rate. This supports the assumption that the extra struck counters were due to multiple scattering and δ rays (the intercept of this line) and to random tracks dependent upon the rate. The net result of the above three effects, after suitably averaging over the actual W and H counter rates, was that pi-mu-atom events which satisfied the trigger represented $(85.8 \pm 0.9)\%$ of all atom events which traversed the spectrometer.

VII. SYSTEMATIC ERRORS

Systematic errors in the calculation of the ratio of the pi-mu-atom acceptance to the $K_{\mu 3}$ acceptance stemmed from uncertainties in the values of various parameters used in the Monte Carlo simulation of the experiment and

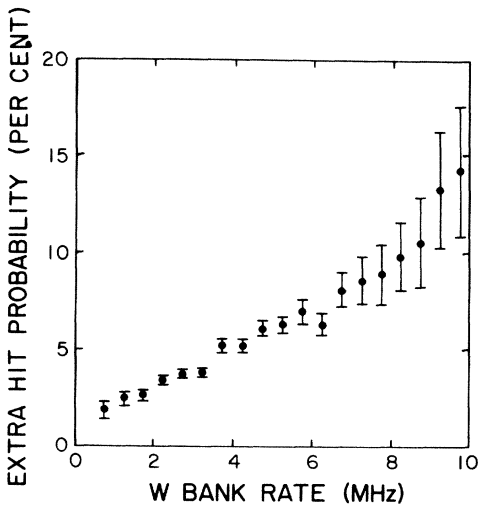

FIG. 26. Measured probability of an extra hit in the W counter bank, as a function of the (separately) measured singles rate in that bank.

in the analysis of data and Monte Carlo events. We examined a number of possible sources of systematic error by varying the Monte Carlo input parameters and studying the resulting change in the calculated acceptance.

As noted above, we adjusted the shape of the K_L^0 momentum spectrum at the target in the Monte Carlo simulation until the reconstructed K_L^0 momentum spectrum agreed with the data, as shown in Fig. 23 for $K_{\mu 3}$ events. Since the measurements of K_S^0 production by Skubic *et al.*[21] did not extend below Feynman x of 0.2, the extrapolation of the spectrum based upon their parametrization of the invariant differential cross section was assumed to be unreliable below 60 GeV/c. However, variations in the integral of the K_L^0 flux below 60 GeV/c of up to $\pm 20\%$ led to changes in the pi-mu-atom to $K_{\mu 3}$ acceptance ratio of only $\pm 1.2\%$. Changes in the shape of the entire spectrum also had little effect on the acceptance ratio. We concluded that the systematic error on our measurement of the branching ratio was 1.5% from this source.

The $K_{\mu 3}$ acceptance had a marked dependence on the values of the $K_{\mu 3}$ form factors $\xi(0)$ and λ_+. In general, larger values of $\xi(0)$ tend to increase the number of events along the Dalitz-plot border where the pion and muon have a small opening angle. Larger values of λ_+ lower the average pion energy. Both of these effects increase the population of the Dalitz plot in the region where our $K_{\mu 3}$ acceptance was highest. The acceptance varied by $\pm 3.5\%$ over $\lambda_+ = 0.034 \pm 0.005$ and by $\pm 1.9\%$ over $\xi(0) = -0.11 \pm 0.09$. However, one must keep in mind that the correlation $d\xi(0)/d\lambda_+ = -14$ is negative, which results in a smaller net error on the acceptance than would be naively expected. Including the effect of this correlation, we calculated the systematic error on the acceptance to be 2.4%.

The location of the components of the apparatus with respect to the beam was critical in determining the acceptances. The ratio of acceptances was calculated with the components' positions varied within their measured errors. The error on the target location gave a 2.1% error while that on the location of the pipe at 321 m yielded a 0.6% error. All other position measurement errors contributed less than 0.2%.

The field strength of magnet A was determined within 0.4% using $\Lambda^0 \to p\pi$ decays. The pi-mu-atom to $K_{\mu 3}$ acceptance ratio was found to vary by less than 2.1% over that range. The strengths of magnet H and magnet V relative to magnet A were measured to better than 0.3%. By analyzing Monte Carlo–generated events with magnet A's field 0.3% higher and lower than that at which the events were generated, we found that the acceptance ratio varied by less than 1.8%. An overall systematic error of 2.8% on the relative pi-mu-atom to $K_{\mu 3}$ acceptances was attributed to the uncertainties in the magnetic field strengths.

All $K_{\mu 3}$ events were required to have a reconstructed K_L^0 decay vertex within the beam. By imposing this requirement, events were lost due to a combination of vertex position resolution and uncertainty as to the cross-sectional dimensions of the beam. In order to estimate the size of any systematic effect of the decay vertex requirements, the size of the area in which the vertex had to lie was increased by as much as a factor of 2 horizontally and 3 vertically. The ratio of accepted data and Monte Carlo events varied by less than $\pm 0.9\%$ over that range. The measurement of this source of error was complicated by background events, since the background increased as the size of the allowed vertex region was increased. The requirements on the decay vertex of the pi-mu atoms introduced a similar source of systematic error. The total effect of all the decay vertex requirements, including the effect of $K_{\mu 3}$ background, was a systematic error on the ratio R of 1.7%.

TABLE III. Sources of errors on the branching ratio R.

Source	Contribution (%)
Systematic errors	
1. Track finding	2.7
2. $K_{\mu 3}$ background subtraction	0.6
3. Trigger corrections	1.0
4. K_L^0 momentum spectrum	1.5
5. $K_{\mu 3}$ form factors	2.4
6. Apparatus location	2.2
7. Magnetic field strengths	2.8
8. Decay vertex requirements	1.7
Total systematic error	5.7
Total statistical error	8.4
Total error	10.1

Table III summarizes our estimates of the systematic errors. A number of tests were performed to search for other effects. The data were divided into two subsamples according to the longitudinal position of the K_L^0 decay point. The difference between the branching ratio results for decay vertices upstream and downstream of 340 m was less than 3%. A subdivision of the data into five groups of runs by beam solid angle yielded a χ^2 of 4.8 for 4 degrees of freedom, using only the statistical errors. In order to verify the constancy of the data-taking conditions, the ratio of the number of detected e^+e^- pairs to the number of detected $K_{\mu 3}$ decays was monitored run by run. No runs were discarded on this basis.

VIII. RESULTS AND CONCLUSIONS

There were 163 events in the range $0.08 < \alpha < 0.20$ when all atom requirements were imposed. After subtraction of a measured background of 8.2 ± 2.1 events, 154.8 atoms remained in the data sample. A total of 109 469 events, collected concurrently, satisfied all the $K_{\mu 3}$ criteria. Subtracting a background of $(5.2 \pm 0.6)\%$ left 103 734 $K_{\mu 3}$ decays with which to normalize the sample of pi-mu atoms. The ratio of the pi-mu-atom and $K_{\mu 3}$ acceptances was found to be 119.6 (where errors on this ratio are included in the systematic errors). Including the KMU3 trigger prescale factor of 32, the ratio R of the rate of formation of pi-mu atoms to the $K_{\mu 3}$ decay rate was measured to be[29]

$$R=\frac{\Gamma(K_L^0\to(\pi\mu)_{\text{atom}}\nu)}{\Gamma(K_L^0\to\pi\mu\nu)}=(3.90\pm0.39)\times10^{-7}\,. \tag{14}$$

The total systematic error (5.7%) and the total statistical error (8.4%) have been added in quadrature. Using the $K_{\mu3}$ branching fraction of (27.1±0.4)%, we determined the branching fraction for K_L^0 decay into a pi-mu atom and neutrino to be $(1.06\pm0.11)\times10^{-7}$.

Two different foil thicknesses were used in this experiment: 0.020 and 0.035 in. The branching ratio R was measured for each subsample of the data and found to be

$$\begin{aligned}R_{20}&=(4.20\pm0.51)\times10^{-7},\\ R_{35}&=(3.55\pm0.51)\times10^{-7},\end{aligned} \tag{15}$$

where the statistical and systematic errors have been combined. The consistency of these results supports the assumption that pi-mu atoms were dissociated in the foil with 100% probability.

The theoretically predicted value for R is $(4.31\pm0.08)\times10^{-7}$, where the error reflects the (correlated) errors on the $K_{\mu3}$ form factors, λ_+ and $\xi(0)$, used in the calculation. The errors on these same form factors contributed to the error on the experimental measurement of R via the calculation of the acceptance of the apparatus for $K_{\mu3}$ decay. In order to lessen somewhat the dependence of our result on the value of these $K_{\mu3}$ form factors, a ratio of the measured and predicted branching ratios can be formed, yielding the value

$$\frac{R_{\text{experiment}}}{R_{\text{theory}}}=0.905\pm0.091\,, \tag{16}$$

where the calculation of the error has included the effects of cancellations and correlations of terms with form factors. This value is consistent with unity.

A property of pi-mu atoms that affects somewhat the present determination of the branching ratio is the lifetime. In our Monte Carlo simulation, we assumed that the atom lifetime is determined by the pion and muon lifetimes. If we allow the atom lifetime to vary, then the only measurable effect is to change the number of atoms which decay before reaching the foil, and hence alter the number of pi-mu atoms we would expect to detect. The effect is small because atoms typically lived only 8% of a pion lifetime before they were dissociated in the foil. We note, for example, that if we had assumed in our analysis that the atom lifetime was one third the expected value, our measured branching ratio would have increased by 18% to 4.6×10^{-7}.

In conclusion, we have observed 320 examples of the rare decay

$$K_L^0\to\text{pi-mu atom}+\nu$$

and have used a subset to measure the decay rate relative to the decay $K_L^0\to\pi\mu\nu$. The theoretical prediction for this ratio, calculated on the assumption that the interaction between the muon and the pion at small distances is just the Coulomb interaction, is in agreement with our experimental result.

ACKNOWLEDGMENTS

We wish to thank the staffs of the Meson and Computing Departments at Fermilab and of the Physical Sciences Laboratory at the University of Wisconsin for their support. We benefited greatly from the technical and engineering expertise of A. Alexander, D. Ouimette, and D. Porat. This work was supported by the U.S. Department of Energy and the National Science Foundation.

*Present address: Columbia University, New York, New York 10027.
†Present address: Fermilab, Batavia, Illinois 60510.
‡Present address: University of California, Los Angeles, California 90024.
§Present address: Princeton University, Princeton, New Jersey 08544.
**Present address: State University of New York, Stony Brook, New York 11794.
††Present address: Digital Pathways Inc., Palo Alto, California 94303.
‡‡Present address: Independent Programming Associates, Chicago, Illinois 60614.
§§Present address: Rutgers University, Piscataway, New Jersey 08854.

[1]L. L. Nemenov, Yad. Fiz. **16**, 125 (1972) [Sov. J. Nucl. Phys. **16**, 67 (1973)].
[2]R. Coombes *et al.*, Phys. Rev. Lett. **37**, 249 (1976).
[3]A. L. Hall, Ph.D. thesis, Stanford University, 1977.
[4]U. Bar-Gadda and C. F. Cho, Phys. Lett. **46B**, 95 (1973); C. F. Cho, Nuovo Cimento **23A**, 557 (1974); H. M. M. Mansour and K. Higgins, *ibid.* **36A**, 196 (1976); A. Karimkhodzhaev and R. N. Faustov, Yad. Fiz. **29**, 463 (1979) [Sov. J. Nucl. Phys. **29**, 232 (1979)].
[5]R. Staffin, Phys. Rev. D **16**, 726 (1977).
[6]S. H. Aronson *et al.*, Phys. Rev. Lett. **48**, 1078 (1982).
[7]R. D. Cousins, Jr., Ph.D. thesis, Stanford University, 1981; J. F. Greenhalgh, Ph.D. thesis, Stanford University, 1981; D. Hedin, Ph.D. thesis, University of Wisconsin, 1980.
[8]J. D. Bjorken and S. D. Drell, *Relativistic Quantum Mechanics* (McGraw-Hill, San Francisco, 1974), p. 113.
[9]M. K. Prasad, Acta Phys. Pol. **B10**, 635 (1979).
[10]Ching Cheng-rui, Ho Tso-hsiu, and Chang Chao-hsi, Phys. Lett. **98B**, 456 (1981).
[11]Particle Data Group, M. Roos *et al.*, Phys. Lett. **111B**, 1 (1982); see, in particular, pp. 69–76.
[12]H. W. Fearing, E. Fischbach, and J. Smith, Phys. Rev. D **2**, 542 (1970).
[13]E. S. Ginsberg, Phys. Rev. D **1**, 229 (1970).
[14]The theoretical prediction in Ref. 6 used the 1980 Particle Data Group [R. L. Kelly *et al.*, Rev. Mod. Phys. **52**, S82 (1980)] averages $\xi(0)=-0.14\pm0.11$ and $\lambda_+=0.034\pm0.005$,

and did not include the 3.8% correction to the K_L^0 decay rate to pi-mu atoms. The decrease in the error on $\xi(0)$ led to a corresponding decrease in the error on the prediction for R. The 1982 Particle Data Group averages for the form factors (Ref. 11, pp. 73—76) remained unchanged in 1984 [Rev. Mod. Phys. **56**, S111 (1984)]. The discussion in the 1982 edition is more complete.

[15]These numbers are estimates based on calculations using the parametrization of R. T. Edwards *et al.*, Phys. Rev. D **18**, 76 (1978) and measurements made in the M3 beam.

[16]F. H. Middleton, Physical Sciences Laboratory, University of Wisconsin, Internal Report (unpublished).

[17]R. Piccioni *et al.*, Phys. Rev. D **9**, 2939 (1974); also, J. K. Cobb (private communication).

[18]M. J. Shochet *et al.*, Phys. Rev. D **19**, 1965 (1979); also, C. Grosso-Pilcher (private communication).

[19]D. I. Porat and D. A. Ouimette, IEEE Trans. Nucl. Sci. **26**, 209 (1979). The signal PT was true if a pair of nonadjacent struck A counters and a pair of nonadjacent struck B counters could be found such that (1) neither B counter was offset by more than one counter from its counterpart in the A bank, and (2) the number of counters separating the pair in the A bank differed by at most one from the number separating the pair in the B bank.

[20]W. R. Molzon *et al.*, Phys. Rev. Lett. **41**, 1213 (1978); W. R. Molzon, Ph.D. thesis, University of Chicago, 1979.

[21]P. Skubic *et al.*, Phys. Rev. D **18**, 3115 (1978).

[22]Excellent agreement between real and simulated data was obtained only when care was taken to simulate the distributions for (electron energy)/(photon energy) and for electron-positron opening angle. The distributions were obtained from J. W. Motz, H. A. Olsen, and H. W. Koch, Rev. Mod. Phys. **41**, 581 (1969) (formula 3D-1009A), and A. Borsellino, Phys. Rev. **89**, 1023 (1953), respectively. For correction of misprints by Borsellino, see Hart *et al.*, Phys. Rev. **115**, 678 (1959).

[23]Calculation of trident production when the produced pair's energy is large is complicated by screening and finite nuclear size effects. For a review, see A. G. Wright, J. Phys. A **6**, 79 (1973).

[24]R. L. Ford and W. R. Nelson, SLAC Report No. 210, 1978 (unpublished).

[25]J. B. Marion and B. A. Zimmerman, Nucl. Instrum. Methods **51**, 93 (1967).

[26]V. L. Highland, Nucl. Instrum. Methods **129**, 497 (1975).

[27]B. Rossi, *High Energy Particles* (Prentice-Hall, New Jersey, 1952).

[28]A. Astier *et al.*, in *Proceedings of the Aix-en-Provence International Conference on Elementary Particles,* edited by E. Cremieu-Alcan, P. Falk-Vairant, and O. Lebey (C.E.N. Saclay, Gif-sur-Yvette, France, 1961), Vol. 1, p. 227.

[29]This result is slightly changed from the result reported in Ref. 6, $R=(3.88\pm0.41)\times10^{-7}$. The difference is due to the change in world averages of the $K_{\mu3}$ form factors between 1980 and 1982 (see note in Ref. 14 above). The calculation of the acceptance of $K_{\mu3}$ events, and hence the measurement of R, depends on these form factors.